IEEE Access
Multidisciplinary | Rapid Review | Open Access Journal

Received August 1, 2019, accepted August 22, 2019, date of publication August 29, 2019, date of current version September 12, 2019.

Digital Object Identifier 10.1109/ACCESS.2019.2938263

Multi-Color Laser Diode Heterodyned 28-GHz Millimeter-Wave Carrier Encoded With DMT for 5G Wireless Mobile Networks

HUAI-YUNG WANG, CHIH-HSIEN CHENG, CHENG-TING TSAI, YU-CHIEH CHI, AND GONG-RU LIN, (Senior Member, IEEE)

Graduate Institute of Photonics and Optoelectronics, and Department of Electrical Engineering, National Taiwan University, Taipei 10617, Taiwan

Corresponding author: Gong-Ru Lin (grlin@ntu.edu.tw)

This work was supported by the Ministry of Science and Technology, Taiwan, under Grant MOST 106-2221-E-002-152-MY3, Grant MOST 107-2221-E-002-159-MY3, Grant MOST 107-2221-E-002-158-MY3, and Grant MOST 107-2218-E-992-304-.

ABSTRACT By using a multi-color laser diode carrier with orthogonal polarization and single-carrier modulation, the long-reach single-mode fiber (SMF) passive optical network and millimeter-wave wireless access network (WAN) with carrying narrow-band and channelized discrete multitone (DMT) data format at >1 Gbit/s/channel are demonstrated for 5G wireless mobile applications. For fiber wireline transmission from central office to remote node, the multi-color laser diode is directly encoded by DMT with quadrature amplitude modulation (QAM) levels ranged from 64 to 1024, and the total raw data rate of the received DMT can maintain as high as 88 Gbit/s at a limit modulation bandwidth of 9.125 GHz. The allowable data band consisting of 0.07–6 GHz for 1024 QAM, 6–9 GHz for 512 QAM and 9–9.125 GHz for 256 QAM is achieved even after long-reach transmission in 75-km-long SMF spool. For wireless transmission from remote node to user end with 28-GHz millimeter-wave carrier after optical heterodyne, the wireless transmission distance can lengthen up to 10 meters with allowable data capacity optimized to 29.6 Gbit/s with a modulation bandwidth of 4.1 GHz in total. Consequently, the achievable bit-loaded data band is 256 QAM within 0.07–2.5 GHz and 64 QAM within 2.5–4.1 GHz for 5G mobile WAN transmission via horn antenna pair.

INDEX TERMS The fifth generation (5G) access network, multi-color, injection-locked colorless laser diode, optical heterodyne, single-carrier modulation (SCM), orthogonal polarization, millimeter-wave over fiber (MMWoF), DMT, chromatic dispersion.

I. INTRODUCTION

With dramatically increasing demand on high-definition data streaming, live video broadcasting, and virtual/augmented reality services, the fifth-generation (5G) wireless mobile networks are urgently demanded to replace the current 4G infrastructure, which can increase the data rate by 10 times for network users at remote nodes [1]–[4]. The 5G WAN is demanded with large bandwidth for personal user. According to the International Mobile Telecommunications (IMT) standard, the 5G mobile WAN employs the enhanced mobile broadband (eMBB) service with ultrareliable and low latency communications (URLLC) for emerging applications, and involves the machine-type communications (mMTC) which supports a very large number of devices in a small area [5]–[7].

The future 5G communication will provides high-speed connections with data rate up to Gbit/s for end users, which requires the selection of new and suitable bands for data transmission with millimeter-wave (MMW) carriers. Different research groups have proposed potential bands for 5G mobile networks such as 24.25-28.35, 37-40, and 64-71 GHz bands [8]–[12]. In particular, the MMW carrier at 28-39 GHz usually exhibits small transmission loss of 0.01-0.02 dB/km such that the transmission distance will not be strictly limited in free space. In traditional approach, the MMW carrier at remote node (RN) was obtained by employing a MMW local oscillator (LO), which then delivered the data by frequency up-converting it onto the MMW carrier through MMW mixer [13]. Later on, the optoelectronic

The associate editor coordinating the review of this article and approving it for publication was Pallab K. Choudhury.

oscillator (OEO) based on a synthesizer-free technology has emerged for photonic microwave (MW) or MMW carrier synthesis with low single-sided-band phase noise and high spectral purity [14]–[16]. Nevertheless, the complexity of the OEO scheme is still impractical for applying to the 5G wireless mobile network. More recently, the radio-over-fiber (RoF) technology is considered as an alternative candidate for MMW carrier generation via remote heterodyne detection, which synthesizes the MMW carrier with specific frequency by adjusting the wavelength spacing of dual-/tri-color optical source [17], [18].

Since 1998, the remote heterodyne detection of two individual laser diodes was proposed to generate a microwave carrier at 9 GHz [17]. Even though, the peak power of remotely heterodyned MMW carrier inevitably varies with the phase difference between individual optical carriers due to incoherent. Therefore, the mutually injection-locked semiconductor lasers [19] or optical phase-locked loop [17], [20] were successively employed for spectrally synchronizing and purifying the heterodyned MW/MMW carrier. Particularly, the coherent dual-/tri-color optical carrier for remote MMW heterodyne detection was synthesized using double-sided-band modulation via Mach–Zehnder modulator (MZM). When driving the MZM at null bias point with half-frequency LO signal, odd-order sidebands [21] and optical central carrier suppression [22]–[24] can be retrieved at central office (CO), respectively. Although the MMW optical carrier generated via MZM is a suitable solution for MMW-RoF transmission, the data stream still needs to be modulated via up-scaled frequency mixing [25] or external optical modulation [26]. Each case would inevitably induce high insertion loss (typical insertion loss is about 3.9-9 dB for mixer and about 4-7 dB for modulator) to degrade transmission performance. Although the aid of optical amplifier can somewhat compensate the power loss, the signal-to-noise ratio (SNR) of data delivered by the remotely heterodyned MMW carrier is still degraded by introducing an additional intensity noise. To minimize the power budget, a special colorless laser diode is proposed for serving as modulator and amplifier concurrently, which is injection-locked by laser diodes with two highly coherent modes for establishing the remote-node heterodyne MMW-over-fiber link [27]. Most important, when using the optical heterodyne with dual-/tri-mode optical carrier as a synthesis technique, the optical loss is only about 0.2 dB/km for each mode before MMW carrier generation.

In this work, the multi-color laser diode with orthogonally polarized triple modes and single-carrier modulation (SCM) scheme is developed for long-reach SMF transmission and remotely heterodyned synthesis of MMW carrier at 28 GHz. To target for 5G mobile WAN application with demanded channel data capacity of >1 Gbit/s/channel, the narrow-band channelized discrete multitone (DMT) ranged from 64- to 1024-quadrature amplitude modulation (QAM) level with corresponding bandwidth adjusted from 167 to 114 MHz is demonstrated for 75-km optical wireline and 10-m MMW wireless transmissions. Such an orthogonally polarized multi-color optical carrier successfully performs the wired/wireless coverage for future 5G mobile applications.

II. PRINCIPLE AND EXPERIMENTAL SETUP

A. GENERATION OF ORTHOGONALLY POLARIZED TRIPLE MODES OPTICAL CARRIER

The concept for acquiring the orthogonally polarized triple modes optical carrier is illustrated in Fig. 1(a). First, a single-mode polarized light source is generated from a DFBLD. The polarization of single-mode DFBLD output is adjusted to 45-degree deviated from the preferred polarization of the MZM via an in-line polarization controller. Then, the sinusoidal-wave LO signal at frequency of f_0 generated from a LO modulates the 45°-polarized single-mode carrier via the MZM operated at null-biased point with an offset DC bias. The schematic diagram of the orthogonal tri-color carrier based on a MZM is presented in Fig. 1(b).

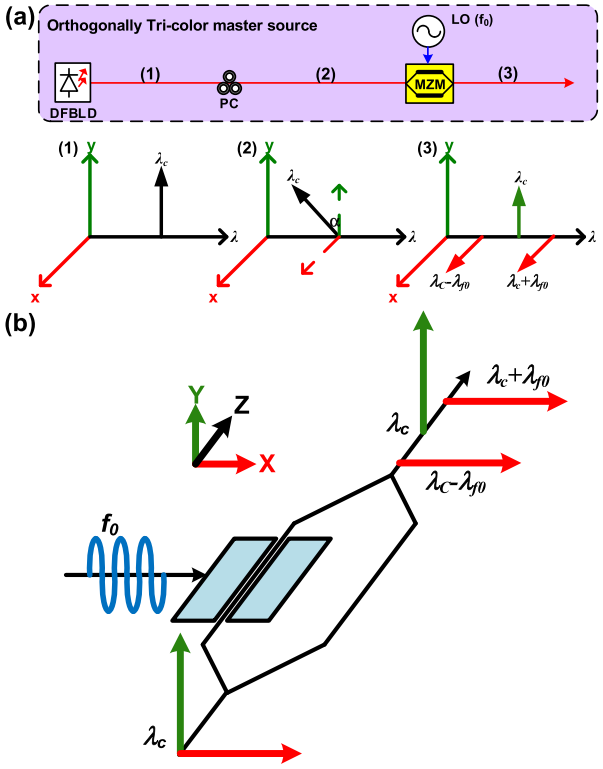

FIGURE 1. A generation process of an orthogonally polarized triple modes master source.

After separating the X and Y polarizations in the MZM, the MZM can only modulate the X-polarized component because the direction of the electric field in the MZM is at X polarization. Under null-biased operation of the MZM, the amplitude of central carrier slightly suppresses to non-linearly generate dual modes ($\lambda_c - \lambda_{fo}$ and $\lambda_c + \lambda_{fo}$). Concurrently, the Y-polarized component (λ_c) just passes through the MZM without modulation. Therefore, the orthogonally polarized triple modes optical carrier is synthesized as expected.

B. SINGLE-CARRIER MODULATION (SCM) OF ORTHOGONALLY POLARIZED MULTI-COLOR OPTICAL CARRIER

In previous work with dual-mode carrier after long-reach fiber transmission, the phase of mode deviates from each other as the carrier modes at different wavelengths still suffer from different chromatic dispersion. To solve this drawback, the orthogonally polarized dual-mode carrier with SCM was subsequently proposed for chromatic dispersion suppression, as shown in Fig. 2(a) [22]. However, the optically heterodyned MMW carrier based on the dual-mode carrier beating is much lower than the traditional approach. Therefore, the proposed tri-color carrier with orthogonal polarization enhances the beating throughput in this work, which not only optimizes the power of beat MMW carrier but also avoids the chromatic dispersion during SMF transmission. The orthogonally polarized tri-color optical carrier with SCM scheme is considered as the optimized approach for improving both wireline and wireless transmission performances of the MMWoF system, as shown in Fig. 2(b).

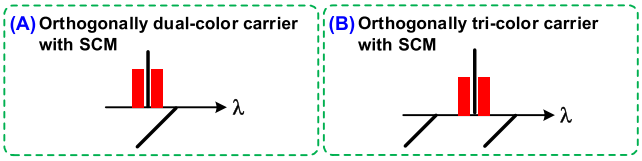

FIGURE 2. The illustration of the (a) orthogonally dual-color optical carrier with SCM and (b) orthogonally tri-color optical carrier with SCM.

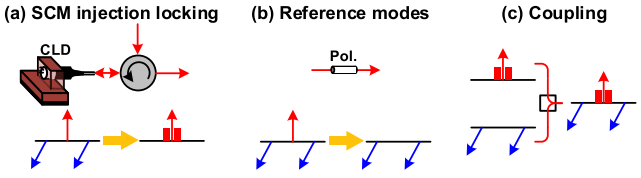

FIGURE 3. A process of a single-carrier CLD with orthogonally polarized injection locking. (a) Master-seeded slave CLD by the orthogonally polarized triple modes master; (b) Filtering the side-mode reference source by a polarizer; (c) Combining the master-seeded slave CLD and the side-mode reference source back to the orthogonally polarized multi-color carrier via an optical coupler.

After the generation of orthogonally polarized multi-color optical carrier, the master source is first split into two paths via a polarized optical coupling element to maintain the orthogonal polarized output separated from one another and achieve SCM via the injection into a mode selective slave colorless laser diode (CLD), as shown in Fig. 3. By directly injecting into the CLD through a circulator, the CLD cavity waveguide design only supports the TE polarization. Only the TE polarized component will survive even if the input source is an orthogonally polarized multi-color carrier. After aligning the polarization between the CLD and the central carrier of triple modes master, the TE-polarized central carrier of the master is locked and modulated by slave CLD to carry the DMT data stream, as shown in Fig. 3(a). Another branch of the coupler output leaves only TM-polarized side modes as a reference source via a high-extinction polarizer, as shown in Fig. 3(b). After performing the SCM for the TE-polarized central carrier, the master-seeded slave CLD output is combined with the side mode reference via another optical coupler to resume back the orthogonally polarized multi-color carrier with SCM, as shown in Fig. 3(c).

C. LONG-REACH-WIRELINE/SHORT-REACH-WIRELESS ACCESS DATA LINK BASED ON THE ORTHOGONALLY POLARIZED MULTI-COLOR OPTICAL AND 28-GHz MMW CARRIERS

The testing bench of a 28-GHz MMW 5G WAN link with an SCM carrier with orthogonally polarized triple modes is illustrated in Fig. 4. To approach SCM on central carrier, a partial power of the triple modes master with orthogonal polarization was coupled into the laser diode modulator for TE-mode injection-locking and direct DMT encoding, whereas the dual TM sidebands were entirely eliminated in the laser diode modulator to achieve SCM operation. To meet the demand of channelization at personal user end for the proposed 5G transmission standards, the DMT data stream with adjusted bandwidth was synthesized from a data generator (Tektronix, 70001A). To maximize the modulation depth in the CLD, the amplitude of generated DMT data was further enlarged with a low-noise amplifier (LNA, picosecond, 5866).

The laser diode modulator also served as an optical amplifier, and its SCM output was combined with the orthogonally polarized side-modes filtered by polarizer to resume back the multi-color carrier with SCM for long-reach SMF transmission. For wireline transmission in SMF with controlled dispersion, the encoded DMT data is received by a photodetector (PD, Nortel, PP-10G) and amplified by a LNA (New focus, 1422). The waveform of the received DMT data is captured by a digital signal analyzer (DSA, Tektronix 71604C) for decoding analysis in a homemade MATLAB program. For remote optical heterodyne, the multi-color polarization recovered from orthogonal to parallel such that the 28-GHz MMW carrier with frequency up-converted DMT data can be synthesized by a high-speed PD (u2t, XPVD2020R) and amplified by a power amplifier (PA, Quinstar, QLW-24403336). After 10-m free-space transmission through a pair of antenna (A-INFO, LB-22-20), frequency down-conversion by a mixer (Quinstar, QMB-FBFBAS) and power amplification via a LNA (New focus, 1422), the DMT data is received by the same DSA and MATLAB program.

D. SCM OF ORTHOGONALLY POLARIZED MULTI-COLOR SOURCE WITH CHANNELIZED DMT FOR MULTIUSER APPLICATION

To meet the demand on the 5G mobile wireless link in which the raw data rate within a limited bandwidth is requested beyond 1 Gbit/s, the bandwidth ranged from 166 to 114 MHz is set to carry the high-level (from 64- to 1024-QAM) DMT data, and the illustration of the DMT is shown in Fig. 5. As the finite frequency response of slave CLD degrades the modulation throughput with a negative slope, the DMT data

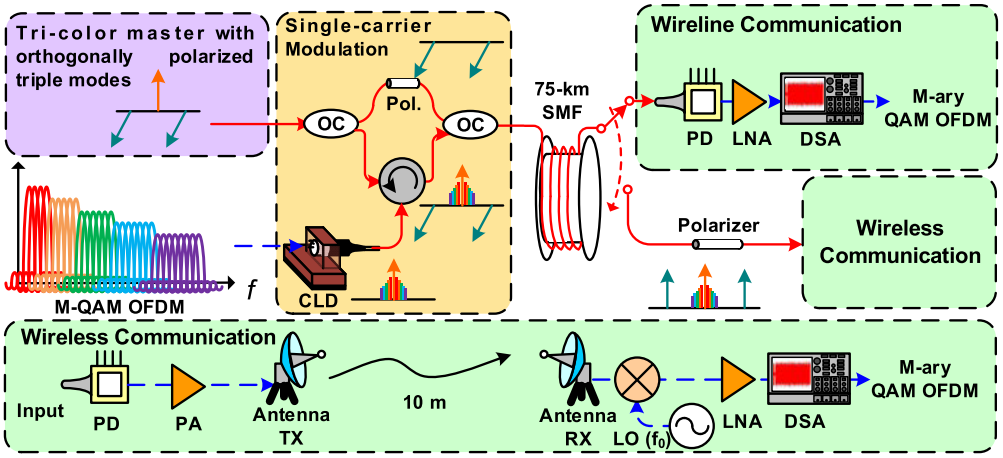

FIGURE 4. Schematic diagram of 28-GHz long-reach MMWoF based on orthogonally polarized multi-color with SCM for combining wireline/wireless transmission.

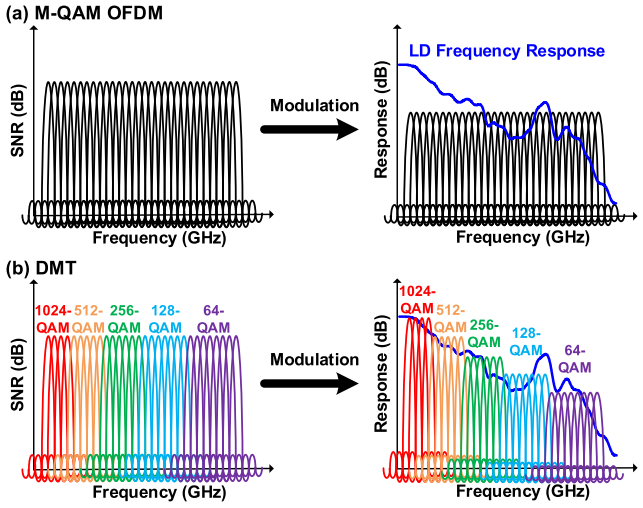

FIGURE 5. Illustration of wideband M-QAM OFDM and DMT onto a finite modulation bandwidth.

encoded at different sub-bands is employed for efficiently increasing the total transmission capacity [28], [29]. At first, a broadband M-QAM OFDM data generated by a 54-GSa/s AWG is used as reference signal to test the channel response, which modulates on the CLD to acquire the SNR response for all subcarriers. In our work, the used bit-loading algorithm does not consider with the power allocation to simplify the decoding procedure [30]. At first, the error vector magnitude (EVM) is analyzed from the received data stream. The relationship among EVM, SNR and bit error rate (BER) is simulated via Monte Carlo method by Shafik *et al.* [31]. The SNR of the *i*th DMT subcarrier is calculated using the following equation:

$$SNR_i = \frac{P_i}{|S_r(i) - S_t(i)|^2} \approx \frac{1}{EVM_i^2}, \tag{1}$$

where $S_r(i)$ denotes the received and normalized *i*th DMT subcarrier, which is corrupted by channel response and noise; $S_t(i)$ the ideal normalized constellation point of the *i*th subcarrier; and P_i the received power of the *i*th DMT subcarrier. Furthermore, the BER of the DMT data is estimated by using the following equation with the relationship between the QAM level and bit number which is expressed by $M=2^n$ with n denoting the bit number [32]

$$BER_{threshold} \geq \frac{2(1-\frac{1}{\sqrt{2^n}})}{n} \times \left\{ erfc\left[\sqrt{\frac{3SNR_i}{2(2^n-1)}}\right] + erfc\left[3\sqrt{\frac{3SNR_i}{2(2^n-1)}}\right]\right\} \tag{2}$$

As applying a FEC criterion with 7% overhead, the BER threshold is 3.8×10^{-3}.

The block diagram of the homemade DMT coding/decoding program is shown in Fig. 6. At first, a pseudo-random bit sequence (PRBS) data with a pattern length of $2^{15}-1$ was mapped onto M-QAM symbols and was arranged in the time-frequency transformation matrix with the FFT size. Note that the M-QAM symbols in the time-frequency transformation matrix are arranged with Hermitian symmetry to obtain a real-valued DMT time-domain waveform after IFFT. After the parallel-to-serial process, cyclic prefix (CP) enabled guard intervals with length of 7% were inserted into each DMT symbol in the DMT time-domain waveform to prevent the inter-symbol-interference after transmission. And then, a training symbol (TS) produced by the 4-QAM data format was further added in the front of the DMT waveform, which was used to find the start point and examine the channel response of the delivered DMT data at the receiving end. At the receiving end, the channel response of the delivered DMT data for equalization was examined by the TS. Then, the DMT data was applied by the serial-to-parallel conversion after removing the TS and CP, which was converted to the complex data and remapped to the constellation plot in frequency domain by FFT. After FFT, a zero-forcing equalizer was used to correct the frequency response and phase noise of the DMT data with the estimated channel response. Finally, the EVM, SNR, and BER performances of received

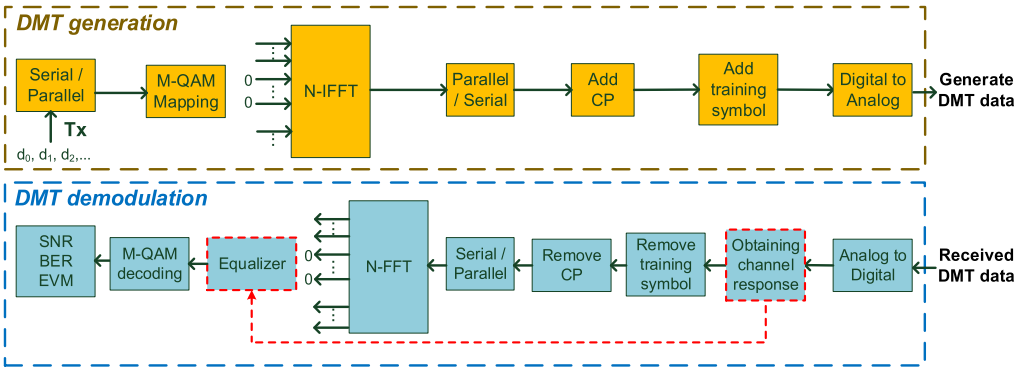

FIGURE 6. The block diagrams of DMT data generation and demodulation.

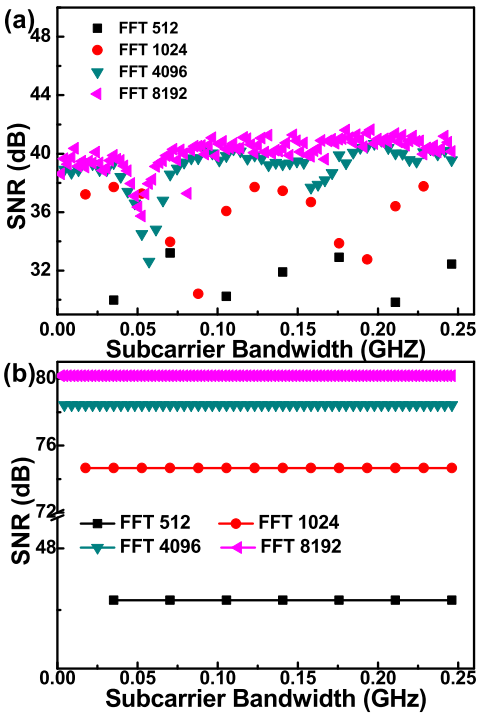

FIGURE 7. The (a) experimental and (b) simulated SNR spectra of the 250-MHz 512-QAM OFDM under different FFT size.

DMT data can thus be obtained by surveying the constellation plots.

III. RESULTS AND DISCUSSION

A. THE PROCESS OF NARROW-BAND M-QAM OFDM DATA GENERATION AND OPTIMIZATION

To maximize the transmission capacity and meet the demand on channel bandwidth for 5G standard, the narrow-band 512-QAM with 250-MHz bandwidth OFDM is synthesized by adjusting the fast Fourier transform (FFT) size in the homemade MATLAB program, as shown in Fig. 7. In principle, the bandwidth of the QAM-OFDM data can be expressed as [33]

$$BW = N_{Subcarrier} \times \frac{Sampling\ rate}{FFT\ size}, \tag{3}$$

where BW denotes the bandwidth of the QAM-OFDM data, $N_{Subcarrier}$ is the number of the subcarriers arranged within the allowable bandwidth. Under a sub-bandwidth of 250 MHz and a total sampling rate of 18 GSa/s, the FFT size is increased from 512 to 8192, and the required $N_{Subcarrier}$ is increased from 7 to 112 due to the reduced subcarrier spacing from 35.16 MHz to 2.2 MHz. When the FFT size is set at 512, the total subcarrier number is only 7 per symbol so that it would suffer from a serious SNR degradation, as shown in Fig. 7(a). In addition, the constellation plot only reveals spare and blurred points with corresponding EVM of 2.9%. With increasing the FFT size from 512 to 8192, the average SNR of the 250-MHz wide 512-QAM OFDM is optimized from 30.9 dB to 39.5 dB. Moreover, the EVM is optimized from 2.9% to 1.1% with dense and clear constellation plots. Nevertheless, the SNR enhancement is saturated even though the SNR can be optimized with increasing FFT size. If the FFT size is increased from 512 to 1024, the average SNR can only be improved up to 4 dB, and the saturation of average SNR is observed with an increment of 1.2 dB by further enlarging the FFT size to 8192. In principle, varying the FFT size will affect the SNR due to the relationship of $SNR = 10^* \log(P_S/P_N)$ with P_S and P_N denoting signal and quantized noise power, respectively. As the noise level of the data is proportional to $10^*\log(N^*_{floor}N_{FFT}/2)$ with a decrement of $10^*\log(2^n/2)$, where N_{floor} and N_{FFT} denote the electrical noise background and the quantization level of the data, respectively [34]. As a result, Fig. 7(b) shows the simulated SNR spectra of the QAM-OFDM data with different FFT sizes by the homemade MATLAB process in our work. The analysis reveals that the average SNR is nonlinearly improved from 46 dB to 80 dB with increasing the FFT size from 512 to 8192. From Fig. 7(a), the experimental result also exhibits the same trend with the simulated one.

Increasing the FFT size from 512 to 8192 at a fixed sampling rate of 18 GSa/s can enlarge the required subcarrier number from 7 to 112 for synthesizing the DMT data format at frequency domain, which concurrently raises the peak-to-average power ratio (PAPR) of the DMT waveform at the specified complementary cumulative distribution function probability of 0.1 after IFFT in time domain, as shown

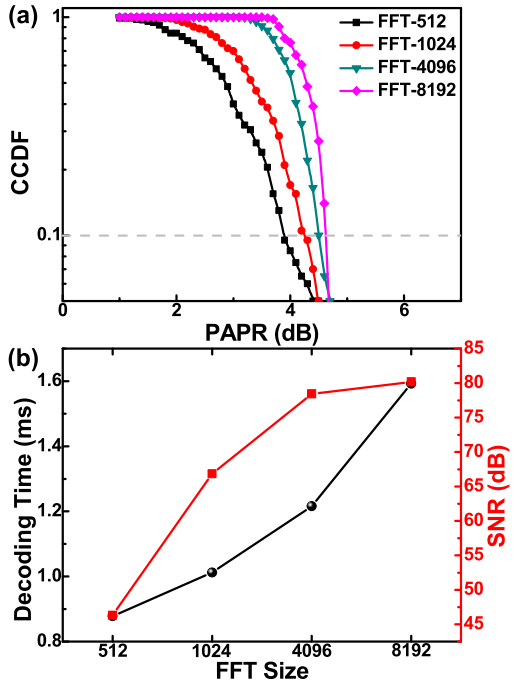

FIGURE 8. (a) The PAPR and (b) required decoding time and average SNR of the DMT data with a single transmission of 32-byte long packet under different FFT size.

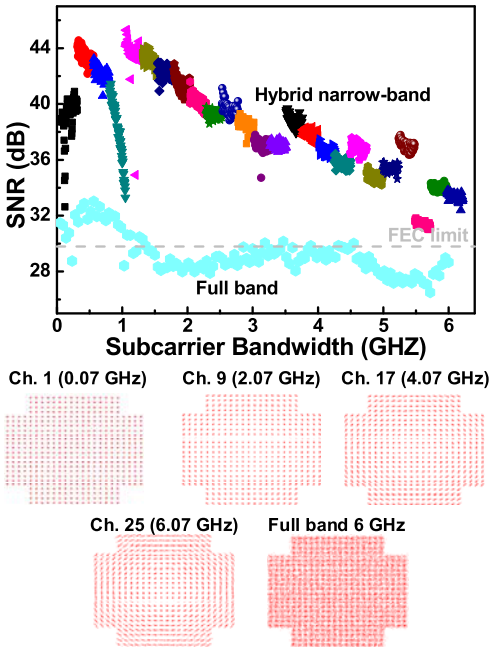

FIGURE 9. The 512-QAM OFDM data based on the channel number of 1 for full-band with channel bandwidth of 6.25 GHz and 25 for narrow-band with channel bandwidth of 250 MHz within the same bandwidth.

in Fig. 8(a). On the other hand, as the complexity of computing for the FFT operation is defined as $O(N \log N)$ with N denoting the data or FFT size, increasing the FFT size from 512 to 8192 will raise the complexity of computing for synthesizing the DMT data format from $O(2^9 \log 2^9)$ to $O(2^{13} \log 2^{13})$. This greatly increases the cost and complexity of the proposed DMT coding/decoding program so as to extend the latency. Fig. 8(b) shows the decoding time of the DMT deciding program and average SNR of the decoded DMT data with the packet length of 32 byte at different FFT sizes. When increasing the FFT size from 512 to 8192, the required decoding time of the DMT deciding program is increased from 0.88 to 1.6 ms, which optimizes the average SNR of the decoded DMT data from 46.3 dB to 80.2 dB. Theoretically, the average SNR of the DMT data can be improved by at least 10 dB with increasing the FFT size from 4096 to 8192. However, the experimental result shows that the improvement of the average SNR after decoding the DMT data is only 3 dB with increasing the FFT size from 4096 to 8192. That is, increasing the FFT size can raise the PAPR of the synthesized DMT data, which leads the peak of the DMT waveform to easily enter the nonlinear modulation region when directly-encoding the CLD. Such a phenomenon inevitably sets an upper limitation when increasing the FFT size. To avoid excessively improving the offline decoding time in program and optimizing the saturation of the decoded DMT data, the optimized FFT size is selected as 4096.

Under the limited modulation bandwidth of 6.25 GHz, the channel number of 1 for full-band with channel bandwidth of 6.25 GHz and 25 for narrow-band with channel bandwidth of 250 MHz are compared with each other and shown in Fig. 9. By setting the start frequency at 70 MHz for both the full-band and hybrid narrow-band data, both cases reveal similar trend caused by finite frequency response of the AWG. Even if the SNR of the hybrid narrow-band 512-QAM OFDM data shows relatively large fluctuation (ranged between 32 dB and 44 dB), its average value is still higher than that of the full-band case as the power of narrow-band data can be effectively enhanced under constant amplitude output in the domain. This essentially enables higher QAM level to be assigned for narrower band data for transmission capacity enlargement when employing the hybrid narrow-band QAM data loading within the same modulation bandwidth. However, the phase noise variation added on the data effectively degrades the constellation plots with blurred points by gradually down-shifting the frequency of the subcarriers.

B. FIBER WIRELINE TRANSMISSION OF ORTHOGONALLY POLARIZED MULTI-COLOR SOURCE WITH SCM OF NARROW-BAND BIT-LOADED M-QAM DMT FOR MULTIUSER APPLICATION

To maximize the transmission capacity and meet the 5G standard with data rate of 1 Gbit/s/ch, the multi-channel M-QAM DMT ranged from 1024-QAM to 256-QAM (with the bandwidth ranged from 114 MHz to 125 MHz) is employed to encode the central carrier of the orthogonally polarized multi-color optical source with SCM scheme. Under the maximal allocated channel number of 91 within allowable bandwidth of 9 GHz, the frequency spectra of the received multi-channel bit-loaded M-QAM DMT data are shown in Fig. 10.

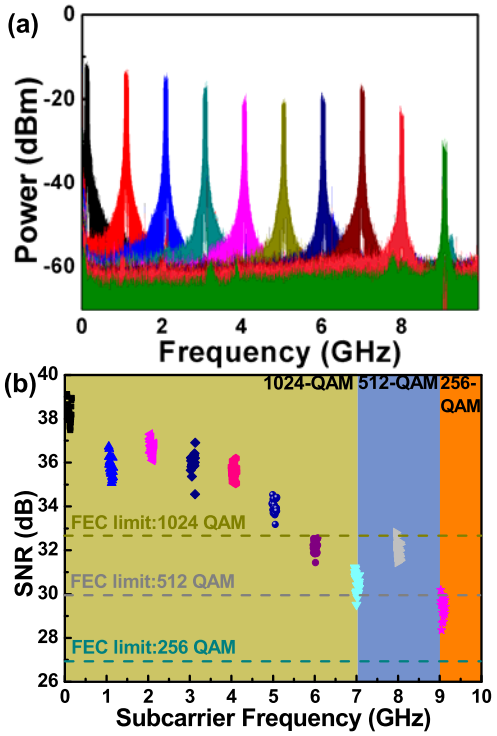

FIGURE 10. The (a) frequency spectra and (b) SNR spectra of the multi-channel DMT data delivered by the orthogonally polarized SCM multi-color optical carriers at 75-km SMF transmissions.

All CNRs of the narrow-band M-QAM DMT data exceed over 30 dB. After decoding, the SNR spectra of narrow-band and bit-loaded M-QAM DMT with their related constellation plots delivered by orthogonally polarized multi-color optical carrier after 75-km DM-SMF transmission are shown for comparison. The SNR of the 1st narrow-band channel reaches 37.5 dB to pass the 1024-QAM FEC criterion, which is degraded with increasing the subcarrier frequency due to the finite frequency response of the slave CLD. The largest channel number which allows the 1024-QAM FEC is up to 60 (with corresponding subcarrier frequency up to 6 GHz). To meet the FEC demanded BER, the 512-QAM format is hired to encode the residual bandwidth from 6 to 9 GHz. As a result, the last (91st) narrow-band channel with 256-QAM format is obtained with an SNR of 28.9 dB.

In more detail, the constellation plots of the narrow-band DMT data at different subcarriers delivered by the orthogonally polarized multi-color source with SCM are illustrated in Fig. 11. At subcarrier bandwidth below 6 GHz, the narrow-band 1024-QAM data successfully passes the FEC criteria with receiving EVMs (or BERs) ranged from 1.3% (or 1.3×10^{-5}) to 2.1% (or 3.2×10^{-3}). The EVM reveals a raising trend as opposed to the SNR by raising the subcarrier frequency as well as channel number, which causes the constellation plots blurred spots of the decoded data associated with high-frequency subcarriers. With increasing the subcarrier frequency over 6 GHz, the narrow-band DMT data can only reach the FEC criteria of up to 512-QAM mapping with corresponding EVMs enlarged from 2.7% to 3.2% and

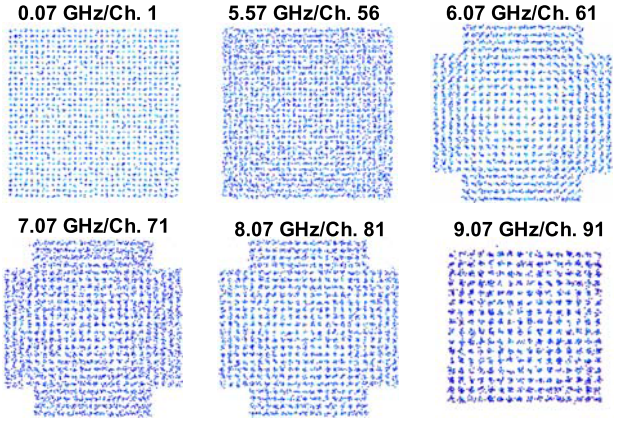

FIGURE 11. The constellation plots of the multi-channel DMT data delivered by the orthogonally polarized SCM multi-color optical carriers at 75-km SMF transmissions.

BER degraded from 9.6×10^{-4} to 9.4×10^{-4}. This result in the maximal channel amount of 90 encodes the 512-QAM covering total bandwidth of 3 GHz (from 6 to 9 GHz). At last channel, the data mapped onto 256-QAM exhibits EVM of 3.6% and BER of 5.8×10^{-4}. Eventually, the total raw data rate of the delivered DMT within 9-GHz bandwidth can extend up to 88 Gbit/s, as composed by 1024-QAM covering 6 GHz, 512-QAM covering 3 GHz and 256-QAM covering 125 MHz (10×6 GHz$+9 \times 3$ GHz$+8 \times 0.125$ GHz).

C. 28-GHz MMW WIRELESS TRANSMISSION OF CHANNELIZED DATA WITH DMT DATA

To maximize the transmission capacity and to meet the demand of channelized data rate under the 5G standard, the multi-channel DMT is also discussed to extend the applicability of the proposed system for MMWoF 5G compatible wireless transmission by the best optical carrier, as shown in Fig. 12. The allowable channel number within 4-GHz bandwidth is 41 with the first channel started from 70 MHz. After 75-km DM-SMF and 10-m free space transmission, the frequency spectra of the received multi-channel and bit-loaded M-QAM DMT data down-converted from 28-GHz MMW carrier generated by the orthogonally polarized multi-color optical source are shown in Fig. 13(a). The peak power of the narrow-band M-QAM DMT is almost 10-dB higher than the broadband case due to the confined gain of the post-amplifier, and the CNRs of all narrow-band M-QAM DMT data exceed over 30 dB. After decoding, the selected SNR spectra of some narrow-band M-QAM DMT data with their related constellation plots are exhibited in Figs. 13(b) and 13(c). The SNR of 27 dB for the 1st channel can pass the 256-QAM FEC criterion with EVM of 4.5% and the BER of 3.6×10^{-3}. In contrast, the average SNR is decreased from 27 dB to 21.6 dB when increasing the subcarrier frequency from 70 MHz to 2.57 GHz, as both the frequency responses of the slave CLD and the mixer with a 3-dB bandwidth are limited at 4.5 GHz. Therefore, the accessible QAM level which can meet the FEC criterion is 64 when subcarrier frequency is set beyond 2.57 GHz.

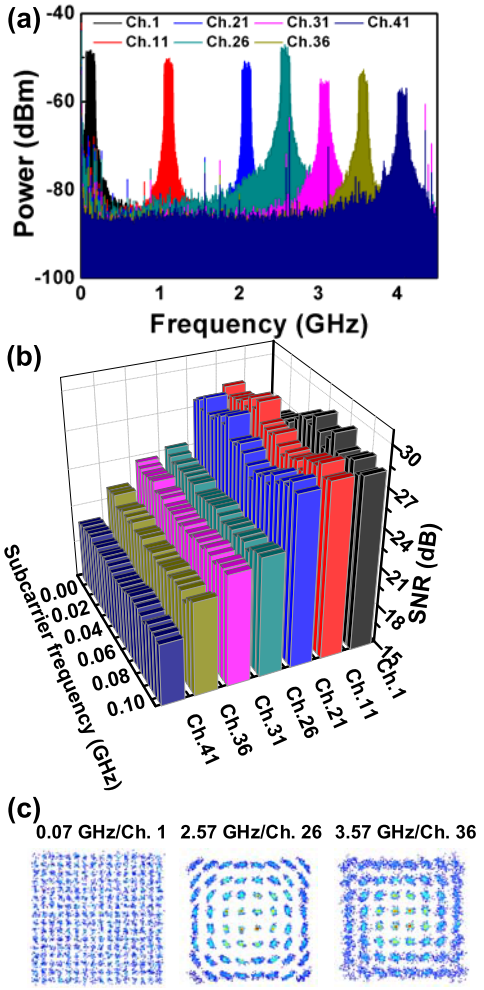

FIGURE 12. The (a) frequency, (b) the SNR spectra and (c) the constellation plots of the multi-channel DMT data delivered by the orthogonally polarized and SCM multi-color source for 5G compatible MMWoF wireless transmission.

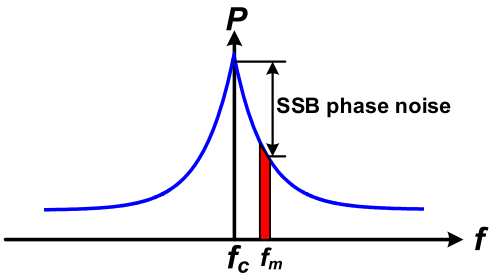

FIGURE 13. Schematic diagram of the phase noise spectrum of the MMW carrier.

The last 41st channel with 64-QAM format provides average SNR of 21.2 dB with EVM of 8.7% and BER of 3.5×10^{-3}. As a results, the whole channels give the total raw data rate of the bit-loaded M-QAM DMT data as 8 (for 256 QAM) × 2.5 GHz + 6 (for 64 QAM) × 1.6 GHz = 29.6 Gbit/s.

Typically, the output frequency spectrum of the AWG and non-ideal synthesizer would contain phase noise in frequency domain as well as timing jitter in time domain. The phase noise spectrum can be plotted as the noise power ratio defined as the noise power (to the central carrier power) in a 1-Hz bandwidth versus offset frequency, as shown in Fig. 13.

The timing jitter $\sigma(f)$ can be obtained by integrating the single-sideband (SSB) phase noise spectrum [35]

$$\sigma(f) = \frac{\left\{2\int_{f_L}^{f_H}\left[(10^{L_n(f)/10} - 10^{L_1(f)/10})/(n^2-1)\right]df\right\}^{1/2}}{2\pi f_R}, \tag{4}$$

where f_R is the repetition rate, $L_n(f)$ is the SSB phase noise of the nth harmonic frequency component of the MMW carrier, n is the harmonic number of the SSB phase noise, and f_L and f_H are the lower and higher limits of integration. After integral over the whole phase noise spectrum, the relative timing jitter added to the data stream carried by each DMT subcarrier can degrade the SNR and BER performance. The relationship between SNR and jitter is given by

$$SNR = 20\log\left(\frac{1}{2\pi\sigma(f)}\right). \tag{5}$$

Finally, the BER performance can be obtained by Eq. (2). After 10-m free space transmission, the phase noise is further increased by electrical amplification and unstable because the channel response of the wireless network is time dependent. The timing jitter is increased to affect the SNR of the transmitted DMT data degradation. Comparing with the structures shown in Refs. [36] and [37], the only difference is the injection-locked colorless laser diode with polarization control for replacing the external modulator. It is worth noting that modulating a data with an external modulator suffers from large power loss and device cost. To compromise the loss for long-reach transmission, an additional optical amplifier is usually required for power compensation. In this point of view, we propose an alternative approach with using a colorless laser diode as both the modulator and the optical amplifier. This merits our propose long-reach MMWoF network a good potential as compared to others. In the proposed link, the polarization controller can be replaced by a segment of polarization maintaining fiber (PMF) with its distance even shorter than the SMF built in the polarization controller, which preserves the fiber-based link more stable than the current setup.

IV. CONCLUSION

To enable the oscillator-free millimeter-wave over fiber link for beyond 5G wireless high-speed access network (WAN) application at next generation, the multi-color laser diode encoded with narrow-band bit-loaded M-QAM DMT is proposed for remotely optical heterodyne of 28-GHz millimeter-wave carrier synthesis. This is approached by employing the orthogonally polarized multi-color laser diode with SCM encoded narrow-band M-QAM DMT data at >1 Gbit/s/channel.

After increasing the FFT size from 512 to 8192, the average SNR of the 250-MHz wide 512-QAM OFDM is optimized from 30.9 dB to 39.5 dB. Under the modulation bandwidth

of 6.25 GHz, the narrow-band bit-loaded M-QAM DMT data exhibits high average SNRs (ranged between 32 dB and 44 dB) which reveals a similar trend than the full-band M-QAM OFDM modulation with an average SNR of only 29.8 dB. Note that the performance of the narrow-band data can be effectively enhanced under constant amplitude output in the time domain.

For the fiber wireline link with DMT data format, the total raw data rate is increased up to 88 Gbit/s under a limited modulation bandwidth of 9.125 GHz (6 GHz for 1024 QAM, 3 GHz for 512 QAM and 0.125 GHz for 256 QAM) after 75-km SMF transmission. For the 28-GHz MMW wireless link over 10 meters via horn antenna pair, the transmission capacity is optimized to 29.6 Gbit/s within allowable bandwidth of 4.2 GHz (256-QAM/2.5-GHz+64-QAM/1.6-GHz). These results declare the applicability of the multi-color laser diode heterodyne technique with DMT data encoding for future 5G MMW mobile WAN links.

ACKNOWLEDGMENT

This work was supported by the Ministry of Science and Technology, Taiwan, R.O.C., under grants MOST 106-2221-E-002-152-MY3, MOST 107-2221-E-002-159-MY3, MOST 107-2221-E-002-158-MY3 and MOST 107-2218-E-992-304-.

REFERENCES

[1] S. Hossain, "5G wireless communication systems," *Amer. J. Eng. Res.*, vol. 2, no. 10, pp. 344–353, 2013.

[2] A. Liu, H. Yin, B. Wu, and Z. Zhou, "Flexible TWDM–RoF system with good dispersion tolerance for downlink and uplink based on additional SCS," *Appl. Opt.*, vol. 57, no. 31, pp. 9432–9438, Nov. 2018.

[3] B. G. Kim, S. H. Bae, H. Kim, and Y. C. Chung, "RoF-based mobile fronthaul networks implemented by using DML and EML for 5G wireless communication systems," *J. Lightw. Technol.*, vol. 36, no. 14, pp. 2874–2881, Jul. 15, 2018.

[4] M. Steeg, N. J. Gomes, A. A. Juarez, M. Kosciesza, M. Lange, Y. Leiba, H. Mano, H. Murata, M. Szczesny, and A. Stohr, "Public field trial of a Multi-RAT (60 GHz 5G/ LTE/WiFi) mobile network," *IEEE Wireless Commun.*, vol. 25, no. 5, pp. 38–46, Oct. 2018.

[5] R. M. Borges, T. R. R. Marins, M. S. B. Cunha, H. R. D. Filgueiras, I. F. da Costa, R. N. da Silva, D. H. Spadoti, L. L. Mendes, and A. C. Sodré, "Integration of a GFDM-based 5G transceiver in a GPON using radio over fiber technology," *J. Lightw. Technol.*, vol. 36, no. 19, pp. 4468–4477, Oct. 1, 2018.

[6] A. Liu, H. Yin, and B. Wu, "High-efficient full-duplex WDM-RoF system with sub-central station," *Opt. Commun.*, vol. 414, no. 4, pp. 72–76, May 2018.

[7] J. Kim, M. Sung, E.-S. Kim, S.-H. Cho, and J. H. Lee, "4×4 MIMO architecture supporting IFoF-based analog indoor distributed antenna system for 5G mobile communications," *Opt. Express*, vol. 26, no. 22, pp. 28216–28227, Oct. 2018.

[8] M. Sung, S.-H. Cho, J. Kim, J. K. Lee, J. H. Lee, and H. S. Chung, "Demonstration of IFoF-based mobile fronthaul in 5G prototype with 28-GHz millimeter wave," *J. Lightw. Technol.*, vol. 36, no. 2, pp. 601–609, Jan. 15, 2018.

[9] C.-Y. Lin, Y.-C. Chi, C.-T. Tsai, H.-Y. Wang, and G.-R. Lin, "39-GHz millimeter-wave carrier generation in dual-mode colorless laser diode for OFDM-MMWoF transmission," *IEEE J. Sel. Topics Quantum Electron.*, vol. 21, no. 6, Nov./Dec. 2015, Art. no. 1801810.

[10] E. Martin, C. Browning, L. Barry, A. Farhang, L. Doyle, M. H. Hoang, M. John, and M. Ammann, "28 GHz 5G radio over fibre using UF-OFDM with optical heterodyning," in *Proc. Int. Top. Meeting Microw. Photon. (MWP)*, Beijing, China, 2017, pp. 1–4.

[11] U. Habib, M. Steeg, A. Stöhr, and N. J. Gomes, "Single radio-over-fiber link and RF chain-based 60 GHz multi-beam transmission," *J. Lightw. Technol.*, vol. 37, no. 9, pp. 1974–1980, May 1, 2019.

[12] C.-T. Tsai, C.-C. Li, C.-H. Lin, C.-T. Lin, S. Chi, and G.-R. Lin, "Long-reach 60-GHz MMWoF link with free-running laser diodes beating," *Sci. Rep.*, vol. 8, Sep. 2018, Art. no. 13711.

[13] C. Lim, A. Nirmalathas, D. Novak, R. Waterhouse, and G. Yoffe, "Millimeter-wave broad-band fiber-wireless system incorporating baseband data transmission over fiber and remote LO delivery," *J. Lightw. Technol.*, vol. 18, no. 10, pp. 1355–1363, Oct. 2000.

[14] Y.-C. Chi and G.-R. Lin, "A *Q*-factor enhanced optoelectronic oscillator for 40-Gbit/s pulsed RZ-OOK transmission," *IEEE Trans. Microw. Theory Techn.*, vol. 62, no. 12, pp. 3216–3223, Dec. 2014.

[15] Y. Wang, Y. Shan, C. Du, Y. Li, Y. Wang, D. Wang, W. Dong, and X. Zhang, "Wideband tunable up-converting optoelectronic oscillator based on gain–loss compensation technology and stimulated Brillouin scattering," *Opt. Quantum Electron.*, vol. 51, no. 43, pp. 1–12, Feb. 2019.

[16] Y.-C. Chi, H.-Y. Wang, C.-H. Cheng, and G.-R. Lin, "40 Gbit/s pulsed RZ-BPSK transmission with a 40 GHz self-pulsated distributed feedback laser diode Mach–Zehnder intensity modulator link," *J. Opt. Commun. Netw.*, vol. 50, no. 8, pp. 610–618, Jul. 2014.

[17] U. Gliese, T. N. Nielsen, S. Nørskov, and K. E. Stubkjær, "Multifunctional fiber-optic microwave links based on remote heterodyne detection," *IEEE Trans. Microw. Theory Techn.*, vol. 46, no. 5, pp. 458–468, May 1998.

[18] J. Yao, "Microwave photonics," *J. Lightw. Technol.*, vol. 27, no. 3, pp. 314–335, Feb. 1, 2009.

[19] L. Goldberg, H. F. Taylor, J. F. Weller, and D. M. Bloom, "Microwave signal generation with injection-locked laser diodes," *Electron. Lett.*, vol. 19, no. 13, pp. 491–493, Jun. 1983.

[20] A. J. Seeds and K. J. Williams, "Microwave photonics," *J. Lightw. Technol.*, vol. 24, no. 12, pp. 4628–4641, Dec. 2006.

[21] R. Bhatia, S. Prakash, and E. Saini, "Performance improvement of 60-GHz wireless optical systems with reverse-parallel hybrid modulation scheme," *Int. J. Commun. Syst.*, vol. 32, Jan. 2019, Art. no. e3848.

[22] H.-Y. Wang, Y.-C. Chi, and G.-R. Lin, "Remote beating of parallel or orthogonally polarized dual-wavelength optical carriers for 5G millimeter-wave radio-over-fiber link," *Opt. Express*, vol. 24, no. 16, pp. 17654–17669, Aug. 2016.

[23] S. K. Mohapatra, B. R. Swain, N. Pati, and A. Pradhan, "Road towards mili meter wave communication for 5G network: A technological overview," *Trans. Machine Learn. Artif. Intell.*, vol. 2, no. 3, pp. 48–60, 2014.

[24] C.-Y. Lin, Y.-C. Chi, C.-T. Tsai, H.-Y. Chen, M. Xu, G.-K. Chang, and G.-R. Lin, "Millimeter-wave carrier embedded dual-color laser diode for 5G MMW of link," *J. Lightw. Technol.*, vol. 35, no. 12, pp. 2409–2420, Jun. 15, 2017.

[25] S.-H. Fan, C. Liu, and G.-K. Chang, "Heterodyne optical carrier suppression for millimeter-wave-over-fiber systems," *J. Lightw. Technol.*, vol. 31, no. 19, pp. 3210–3216, Oct. 1, 2013.

[26] J. Zhang, J. Yu, N. Chi, F. Li, and X. Li, "Experimental demonstration of 24-Gb/s CAP-64QAM radio-over-fiber system over 40-GHz mm-wave fiber-wireless transmission," *Opt. Express*, vol. 21, no. 22, pp. 26888–26895, Oct. 2013.

[27] C.-T. Tsai, Y.-C. Chi, and G.-R. Lin, "Destructively interfered beating dual-mode VCSEL for carrierless MMW fiber-wireless access link with suppressed RF fading," *IEEE J. Sel. Topics Quantum Electron.*, vol. 23, no. 6, Nov./Dec. 2017, Art. no. 1700309.

[28] C. Vagionas, S. Papaioannou, G. Kalfas, N. Pleros, N. Argyris, K. Kanta, N. Iliadis, G. Giannoulis, D. Apostolopoulos, and H. Avramopoulos, "A six-channel mmWave/IFoF link with 24 Gb/s capacity for 5G fronthaul networks," in *Proc. Int. Top. Meeting Microw. Photon. (MWP)*, Toulouse, France, 2018, pp. 1–4.

[29] C. Vagionas, S. Papaioannou, N. Argyris, K. Kanta, N. Iliadis, G. Giannoulis, D. Apostolopoulos, H. Avramopoulos, C. Caillaud, H. Debregeas, G. Kalfas, and N. Pleros, "A 6-Band 12 Gb/s IFoF/V-band fiber-wireless Fronthaul link using an InP externally modulated laser," in *Proc. Eur. Conf. Opt. Commun. (ECOC)*, Rome, Italy, 2018 pp. 1–3.

[30] D. Bykhovsky and S. Arnon, "An experimental comparison of different bit-and-power-allocation algorithms for DCO-OFDM," *J. Lightw. Technol.*, vol. 32, no. 8, pp. 1559–1564, Apr. 15, 2013.

[31] R. A. Shafik, S. Rahman, and A. H. M. R. Islam, "On the extended relationships among EVM, BER and SNR as performance metrics," in *Proc. ICECE*, Dec. 2006, pp. 408–411.

[32] J. Lu, K. B. Letaief, J. C.-I. Chuang, and M. L. Liou, "M-PSK and M-QAM BER computation using signal-space concepts," *IEEE Trans. Commun.*, vol. 47, no. 2, pp. 181–184, Feb. 1999.
[33] Y. Wang, Y. Wang, and Q. Shi, "Optimized signal distortion for PAPR reduction of OFDM signals with IFFT/FFT complexity via ADMM approaches," *IEEE Trans. Signal Process.*, vol. 67, no. 2, pp. 399–414, Jan. 2019.
[34] S. Scholl. *Exact Signal Measurements Using FFT Analysis*. Accessed: Jun. 6, 2019. [Online]. Available: https://kluedo.ub.unikl.de/frontdoor/deliver/index/docId/4293/file/exact_fft_measurements.pdf
[35] Y.-C. Chi and G.-R. Lin, "A self-started laser diode pulsation based synthesizer-free optical return-to-zero on–off-keying data generator," *IEEE Trans. Microw. Theory Techn.*, vol. 58, no. 8, pp. 2292–2298, Aug. 2010.
[36] Z. Cao, J. Yu, L. Chen, and Q. Shu, "Reversely modulated optical single sideband scheme and its application in a 60-GHz full duplex ROF system," *IEEE Photon. Technol. Lett.*, vol. 24, no. 10, pp. 827–829, May 15, 2012.
[37] P. T. Dat, A. Kanno, N. Yamamoto, N. Van Dien, N. T. Hung, and T. Kawanishi, "Full-duplex transmission of Nyquist-SCM signal over a seamless bidirectional fiber–wireless system in W-band," in *Proc. Opt. Fiber Commun. Conf. Exhib. (OFC)*, San Diego, CA, USA, 2019, pp. 1–3.

HUAI-YUNG WANG was born in Taipei, Taiwan, in 1987. He received the B.S. degree from the Department of Applied Materials and Optoelectric Engineering (AMOE), National Chi Nan University (NCNU), Taiwan, in 2010, and the M.S. degree from the Department of Electro-Optical Engineering, National Taipei University of Technology (NTUT), Taipei, in 2012. He is currently pursuing the Ph.D. degree with the Graduate Institute of Photonics and Optoelectronics, National Taiwan University. His research interests include optical communication, including 5G mobile, MMW/RoF, WDM-PON, and OFDM.

CHIH-HSIEN CHENG was born in Taipei, Taiwan, in 1985. He received the B.S. degree from the Department of Electrical Engineering, National Taiwan University of Science and Technology, Taiwan, in 2008, and the Ph.D. degree from the Graduate Institute of Photonics and Optoelectronics, National Taiwan University, in 2016, where he is currently a Postdoctoral Fellow with the Graduate Institute of Photonics and Optoelectronics. His research interests include Si photonic devices, Si-based TFT, Si-QDs-based MOS capacitor, and LED devices.

CHENG-TING TSAI received the B.S. degree in information and telecommunications engineering from Ming Chuan University, Taoyuan, Taiwan, in 2010, the M.S. degree in biophotonics from National Yang-Ming University, Taipei, Taiwan, in 2012, and the Ph.D. degree in photonics and optoelectronics from National Taiwan University, Taipei, in 2017. His research interests include fiber-optic communication systems, radio-over-fiber systems, all-optical millimeter wave generation, digital signals, and laser devices.

YU-CHIEH CHI was born in Taipei, Taiwan, in 1983. He received the B.S. degree from the Department of Electrical Engineering (EE), National Taipei University of Technology (NTUT), Taiwan, in 2005, the M.S. degree from the Department of Electro-Optical Engineering, NTUT, and the Ph.D. degree from the Graduate Institute of Photonics and Optoelectronics, National Taiwan University (NTU), Taipei, in 2012. His research interests include semiconductor laser diodes and optical amplifiers and their application in fiber-optic communication networks with different architectures, including WDM, TDM, PSK, and OFDM.

GONG-RU LIN (S'93–M'96–SM'04) received the B.S. degree in physics from Soochow University, Taipei, Taiwan, in 1988, the M.S. and Ph.D. degree in electro-optical engineering from National Chiao Tung University, Hsinchu, Taiwan, in 1990 and 1996, respectively. He was the Faculty Member of the several universities in Taiwan, from 1997 to 2006. In 2006, he joined as a Full Professor with the Graduate Institute of Photonics and Optoelectronics (GIPO) and the Department of Electrical Engineering, National Taiwan University (NTU), where he is currently a Distinguished Professor and the Director of the GIPO. He has coauthored more than 300 SCI-ranked journal articles, 500 international conference articles, ten book chapters, and 25 invited talks during his research career. In the Laboratory of Fiber Laser Communications and Si Nano-Photonics, his research interests include the fiber-optic communications, the all-optical data processing, the femtosecond fiber lasers, the nanocrystallite Si photonics, the ultrafast photoconductors, and the optoelectronic phase-locked loops. He is a Fellow of the SPIE, IET, IOP, and OSA. He is the current President of the Taiwan Photonics Society. He used to serve as the Chair of the IEEE/Photonics Taipei Chapter.